

X-RAY BURSTS FROM A RANDOM CAVITY EMERGING IN AN INTER-ELECTRODE POLYDISPERSE PLASMA OF NANOSECOND VACUUM DISCHARGE. I. EXPERIMENT: GENERATION, RELEASE, AND TRAPPING OF X RAYS

Yu. K. Kurilenkov,^{1,2*} I. V. Smetanin,² A. V. Oginov,² and I. S. Samoylov¹

¹*Joint Institute for High Temperatures, Russian Academy of Sciences
Izhorskaya str. 13/2, Moscow 125412, Russia*

²*Lebedev Physical Institute, Russian Academy of Sciences
Leninskii Prospect 53, Moscow 119991, Russia*

*Corresponding author e-mail: kurilenkovyuri@gmail.com

Abstract

Earlier, in experiments on DD synthesis in a complex plasma of a nanosecond vacuum discharge (NVD) with a virtual cathode, in parallel, a significant experimental database was accumulated on the output of hard X rays from the inter-electrode ensembles, and a certain correlation was established between the specificity of the X-ray yield and the features of the inter-electrode ensembles of nanoparticles (their density and configuration). In particular, the ability of sufficiently dense inter-electrode ensembles to “trap” X ray radiation (quanta with energies ~ 10 keV or less) was recognized. In this work, we consider and analyze the features of the X-ray yield in experiments on DD synthesis in NVD. We present and discuss the accumulated basic experimental data related to the specifics of the release of hard X rays from the NVD.

Keywords: random cavity, virtual cathode, nanosecond vacuum discharge, spontaneous X-ray burst.

1. Introduction

Compact and powerful sources of fast particles and X rays are in good demand from medicine, biology, and chemistry to materials science and nondestructive testing [1, 2]. In addition to standard X-ray tubes, modern X-ray generators, synchrotron storage rings, multipole wigglers, undulators, and X-ray lasers [3] are used to increase the yield of X rays and to solve specific problems. In particular, because of high gain in the lasing medium, short upper-state lifetimes, and problems associated with construction of mirrors that could reflect X rays, X-ray lasers usually operate without mirrors. Lack of high- Q X-ray cavities forces researchers to consider various nonstandard approaches to providing feedback in this spectral range. Letokhov’s idea of a stochastic resonator [4] has been realized and now is widely used in the visible spectral domain [5–7]. This approach looks very promising in the X-ray spectral range of spectrum; however, X-ray stochastic (random) cavity laser has not yet been implemented.

In recent years, we were investigating, on the basis of a nanosecond vacuum discharge (NVD), an unusual scheme of inertial electrostatic confinement (IEC) [8–13] – this is an IEC scheme with reverse polarity [10]. It contains the injection of electrons into the anode space, the formation of a virtual

cathode (VC) and the corresponding potential well (PW) [14–18]. Ions oscillate in the PW, reaching energies up to ~ 100 keV at the moment of head-on collisions [18]. At the moments of ion collapses at the “bottom” of the PW, both the DD synthesis takes place [15,16] and aneutronic synthesis of $p+^{11}\text{B}$ is possible [17]. The presence of harmonic ion oscillations also partially contributes to the self-support of VC. Therefore, in general, we call confinement in our NVD scheme [16–18] the electrodynamic (or oscillatory) one. Note that the reverse polarity scheme was the first IEC scheme considered theoretically [10].

Further, in order to increase the efficiency of synthesis and avoid the inefficiency of the “beam – beam” scheme in a conventional IEC [8], at the Los Alamos National Laboratory (LANL), it was proposed to inject electrons into the anode space to create a VC and corresponding PW, and create the regime of periodically oscillating plasma spheres (POPS) [11]. However, despite the successful demonstration of POPS for H^{2+} , He^+ , and Ne^+ [12], it was not possible to implement the concept of POPS in further fusion experiments [8,13]. Over a time, it became clear [18] that it was our NVD, in which the VC is very small ($r_{\text{VC}} \sim 0.1$ cm), and the PW is very deep ($\varphi_{\text{PW}} \leq 100$ kV); in the same years [14], it already became as a realization of certain hopes associated with the advantages of POPS [11,12], including the favorable scaling of the fusion power density $P \propto \varphi_{\text{PW}}^2 / r_{\text{VC}}^4$. In the experiment with a cylindrical NVD, ion oscillations were obtained with a frequency of ~ 80 MHz and a PW with a depth of ≤ 100 kV [18]. This provided record values for the fusion power density and made it possible to demonstrate both the DD neutron reaction [14–16] and the possibility of aneutronic proton – boron fusion.

At the same time, in experiments on DD synthesis, in parallel, a significant experimental database was accumulated on the escape of hard X ray from the inter-electrode ensembles of NVD, and a certain correlation was established between the specificity of the X-ray release and the nature of the inter-electrode ensembles of nanoparticles (their density and configuration). In particular, the ability of sufficiently dense inter-electrode ensembles to self-organize and to “trap” X ray (quanta with energies ~ 10 keV or less) was recognized [17]. We devote this paper to the analysis of the features of the X-ray yield in experiments on DD fusion in NVD. An overview of the main accumulated experimental data related to the specifics of the release of hard X rays from the inter-electrode cluster ensembles of the NVD is presented. In the future paper, we propose and discuss a qualitative model of X-ray trapping by the inter-electrode medium; also individual strong bursts of hard X rays, which can be externally similar to random laser flashes [17,21–24] are interpreted.

2. Experiment on DD Synthesis under Plasma Oscillatory Confinement in NVD

In the experiment, we used a modified oscillatory confinement scheme based on a miniature low-energy NVD with a deuterated palladium anode [14–18]. From standard IEC schemes with grid electrodes [8], we switched to a scheme that includes features of the interdisciplinary physics of NVD. In particular, a hollow Al cathode with a conical part and a Pd anode, which was periodically filled with deuterium during electrolysis in heavy water, was used. Such a scheme of IEC with reverse polarity [10] makes it possible to work in a vacuum, where beams of energetic electrons from the cathode are formed when the voltage is applied [15]. The latter, interacting with the deuterated Pd anode, first will create near the anode an erosion plasma containing, among other things, deuterons and deuterium-containing clusters. Second, electron beams, penetrating into the anode space (through the “grid” of thin Pd tubes) and decelerating in its center, form a VC and the corresponding PW. A deep potential well (tens of kV) will

play the role of a microaccelerator, accelerating deuterons from the edges of the well to energies of tens of keV and colliding their head-on fluxes with each other on the discharge axis, i.e., at the “bottom” of the PW [15–18]. Third, last but not least, beams of energetic (~ 50 keV) electrons, interacting with a polydisperse inter-electrode medium and electrodes, generate hard X rays [17].

In this work, the subject of main interest are the features of the generation and release of X rays in the NVD. However, for a clear understanding of what is happening with the generation of X rays, we first describe briefly the experiment on DD fusion in NVD as a whole (a detailed description of the experiment was given earlier in [14–16]). The schematic picture of the experiment is shown in Fig. 1 a, while Fig. 1 b shows an example of a CCD X-ray image of a dense inter-electrode ensemble (the main discharge parameters: $U \sim 70$ kV, $I_{\max} = 1$ kA, $T_{\text{pulse}} = 50$ ns, input energy ~ 1 J). A cylindrical copper anode ($\varnothing = 0.6$ cm) had a packing in the form of a set of thin (0.1 cm in diameter) hollow Pd tubes (from 3 to 13) inserted perpendicular to the end of the anode along its perimeter.

The hollow cylindrical aluminum cathode has a conical part facing the anode. X-ray images of the inter-electrode medium (≥ 1 keV, Fig. 1 b) are recorded by a CCD camera through a hole (pinhole) in a lead plate (0.2 cm thick) covered with 0.1 mm thick aluminum foil. Figure 2, as an illustration of DD synthesis in NVD, shows the CCD of the inter-electrode ensemble and the oscillogram of the X-ray release, in particular, recording the moment of the DD reaction (channel 4) and the neutron peak (channel 2). Channels 1 and 3 (Fig. 2 b) show the X-ray intensity with the maximum sensitivity in the range of about 10 keV. A harder X ray was usually recorded with a photomultiplier PM2 covered with a 0.5 mm thick copper absorber (PM2 and PM4 signals always have an electronic time of delay of ≈ 35 ns compared to the almost instantaneous signals of PIN diodes, channels 1 and 3). Time-of-flight (TOF) measurements of the neutron yield were carried out using PM4 and PM2 located on the same axis with the electrodes at distances of 45 and 90 cm, respectively, from the plasma source (channels 4 and 2 in oscillogram like in Fig. 2 b). Besides of hard Bremsstrahlung and characteristic X rays (the first strong intensity peaks on channels 2 and 4), PM2 can record a well-reproduced signal (the second weak peak) with a delay of about 46.6 ns/m relatively to the moment of DD synthesis. This delay, 46.6 ns/m, is a signature of the presence of DD neutrons with an energy of about 2.45 MeV from the fusion reaction $D + D = n + \text{He}^3$ (their arrival at the scintillator is recorded by the photomultiplier PM2, channel 2).

At the same time, PM4 and PM2 can register the moment of the DD reaction itself by extra X ray due to the spread of fast reaction products, channel 4, as the necessary reference point in time (due to the electronic delay of the PM signal, in real time it coincides with a break in the signal of PIN diodes, channel 3, Fig. 2 b). A change in the experiment of the distance between the plasma source and PM2 (closer – longer) is accompanied by a corresponding shift in the moment of appearance of the neutron peak (earlier – later) [14–16].

Above, only the simplest case is specially shown – a single neutron peak in a low-density (“transparent”) ensemble. However, the physics – acceleration of head-on fluxes of deuterons by the field of a virtual cathode – is repeated in denser stochastic inter-electrode NVD ensembles too [18, 25, 26]. Note that the neutron yield in NVD can vary from shot-to-shot, and amounts to about $10^5/4\pi$ neutrons for “transparent” ensembles (like the regime in Fig. 2) increases to $\sim 10^7/4\pi$ for dense inter-electrode ensembles (of the type shown in Fig. 8 below) by ≈ 1 J of total energy loaded in NVD [15, 16].

Deuterons can oscillate in the PW, reaching energies up to ~ 100 keV at the moment of head-on collisions [16]. At these moments of periodic collapse of deuterons at the PW bottom, DD fusion takes place accompanied by a pulsating neutron yield [18]. The appearance of neutrons at the initial stage of the discharge (dashed arrows in Fig. 2 a) is discussed in detail in [27].

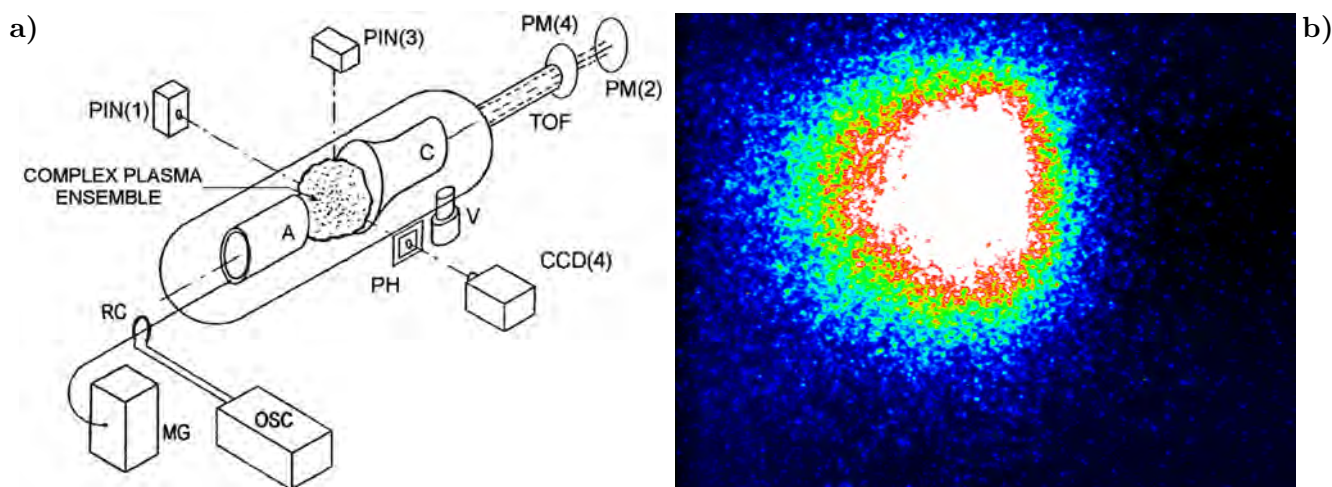


Fig. 1. Schematic of the experiment (a); here, Marks generator (MG), Rogowski coil (R), deuterated anode (A) and hollow cathode (C), photodiodes calibrated in the X-ray range of 1–15 keV (PIN), CCD camera (CCD), pinhole covered with 0.1 mm aluminum foil (PH), photomultipliers (PM-2 and PM-4), oscilloscope (OSC), a tube for time-of-flight measurements (TOF), and vacuum pump (V), and CCD image of dense inter-electrode ensemble (b) practically “trapping” not very hard X-rays, ≤ 10 keV; see text.

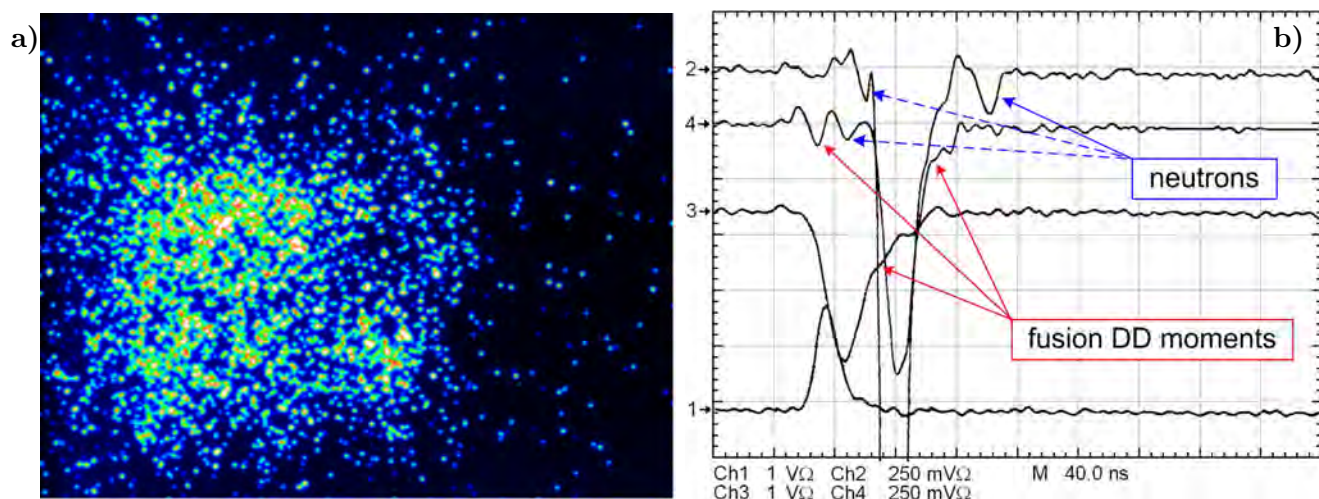


Fig. 2. Dynamics of X-ray yield in mode 1; here, CCD image of a low-density (“transparent”) inter-electrode ensemble (a) and oscillograms (b) of X-ray yield (channels 1–4) and neutrons (channel 2, small peak).

3. Generation, Release, and “Trapping” of X Rays in the Inter-Electrode Medium of NVD

In the experiment with NVD, we can change to some extent the level of X-ray absorption and multiple scattering inside polydisperse inter-electrode ensembles by changing the inter-electrode volume (varying the anode–cathode distance) under approximately constant mass transfer from the anode and also smoothly varying the pressure in the range of $10^{-6} - 10^{-2}$ mbar. If the density of the stochastic cluster ensemble is high and the conditions for diffusion of photons, $\lambda \ll l_{SC} \ll R$, are satisfied, photons can be rescattered in a disordered dense polydisperse medium for a relatively long time before leaving it from

the near-surface region; see also [5, 21–24] (here, λ is the wavelength, l_{SC} is the average mean free of photon in the medium due to scattering, R is the size of the ensemble; $l_{SC} = 1/N_0 Q_S$, where Q_S is the scattering cross-section, N_0 is the bulk density of scattering particles, and $N_0^{-1/3} \gg \lambda$). Experiment shows [17] that dense inter-electrode ensembles in NVD can apparently partially “trap” even relatively hard quanta (~ 10 keV).

Recall that the PM (2) and PM (4) photomultiplier signals (Fig. 2 b) always have a delay time of ≈ 35 ns due to the time of flight of electrons in the PM tube relative to instantaneous signals (channels 1 and 3) synchronized with PIN diodes. Thus, usually for low-density ensembles (Fig. 2 a), the photomultiplier signal (channel 2, photon energy > 20 keV) appears ~ 35 ns later, due to electronic delay with respect to the almost instantaneous signals of PIN diodes (the most sensitive in the range of 3–10 keV, channels 1 and 3 in Fig. 2 b). In this case, in real time, the maxima of the signals on the channels of PIN diodes 1, 3 and PM channels 2, 4 should practically coincide.

Stochastic ensembles of clusters in a vacuum discharge discussed in detail earlier in relation to nuclear DD fusion in an inter-electrode medium [15, 16] are perhaps of interest for attempts to implement some lasing effects [4, 21] in the X-ray range [17]. Depending on the density and characteristic sizes of clusters and nanoparticles in polydisperse ensembles and also depending on the degree of symmetry of the ensembles themselves, different features of the X-ray escape were observed previously [16, 17]. An inhomogeneous dense cluster inter-electrode medium, apparently, can provide a multiple scattering regime close to diffuse one, even for rather hard X-ray quanta less than or of the order of 10 keV [17]. The beginning of the X-ray “trapping” in the inter-electrode ensembles, as their density increases, is illustrated for the regime shown in Fig. 3. (Shown here is an ensemble with a significantly higher density of clusters than for the regime shown in Fig. 2 above.) For the inter-electrode ensemble shown in Fig. 3 a, we can observe the start of the X-ray emission delay inside the medium (quanta are less than or ~ 10 keV, channels 1 and 3 in Fig. 3 b), i.e., actually the diffusion of X rays in the ensemble.

Indeed, the recorded maxima of the signal intensities of the photomultiplier (channel 2) and PIN diodes (channels 1 and 3) approximately coincide in time (Fig. 3 b). But for their correct comparison with each other in real time, the maximum of the hard X ray (channel 2 in Fig. 3 b) must be “shifted” to the left by ~ 35 ns. In other words, a very hard X ray (channel 2) comes out immediately, while the diffusive delay of the X rays recorded by channels 1 and 3 (≤ 10 keV) is about ~ 40 ns (Fig. 3 b). The CCD images of inter-electrode ensembles at higher cluster densities (Fig. 4 a), where the condition of X-ray diffusion $\lambda \ll l_{SC} \ll R$ are satisfied better than for the regime in Fig. 3, have an even lower X-ray emission intensity (Fig. 4 b, channels 1 and 3).

Sometimes such self-organized ensembles, close in shape to a “ball,” are not accompanied by a set of oscillograms at all, if the value of the X-ray intensity in channel 1 turns out to be less than the required trigger U_{trigg} needed to trigger the oscilloscope ($U_{trigg} = 100$ mV). An example of such an ensemble, which is more dense than one in Fig. 3 a was shown earlier in Fig. 1 b. This mode of “trapping” of the X rays immediately followed the mode in Fig. 3, where it did not quite happen yet, and for the mode in Fig. 1 b we have only one CCD image, without oscillograms. Comparison of CCD images clearly shows that the shapes of stochastic ensembles in Figs. 1 b and 3 a are close, but the ensemble density in the latter case is still noticeably lower. Thus, dense ensembles of nanoclusters with an increasing level of self-organization (of the type shown in Figs. 1 b, 3 a, and 4 a; anode of 13 Pd tubes) can partially or noticeably “trap” hard X rays (≤ 10 keV). As a result, due to the diffuse nature of the propagation of photons, the X-ray signal on channels 1 and 3 appears with a delay and also is noticeably weakened due to the losses associated with scattering. But the number of quanta emerging from the skin-layer of the

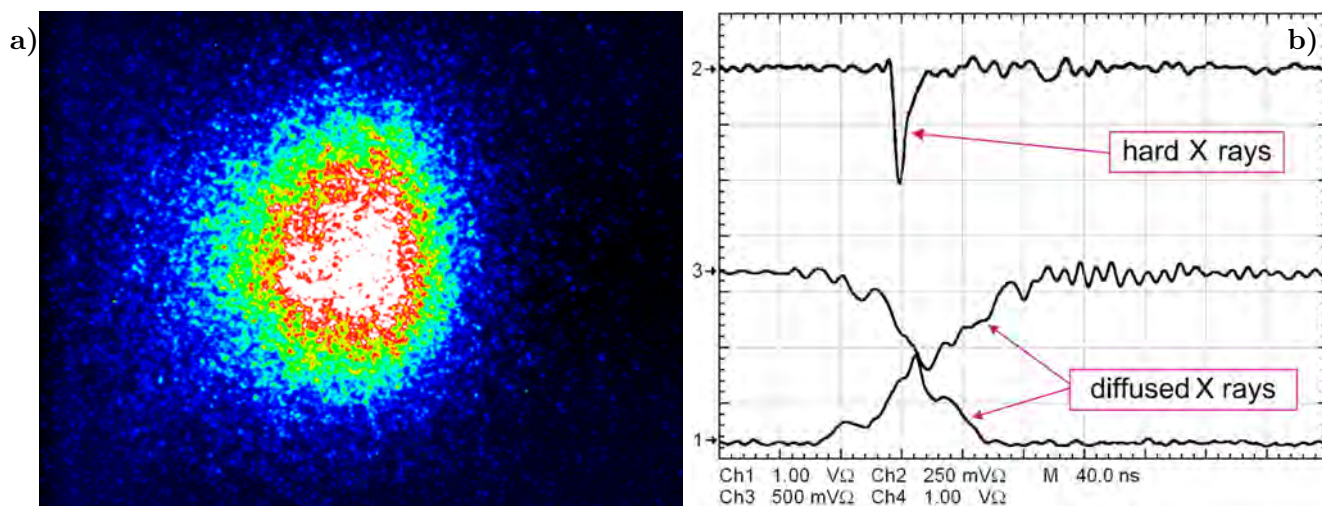


Fig. 3. Dynamics of X-ray yield in mode 2; here, CCD X-ray image of a dense ensemble of nanoparticles, in which diffusion of X-ray photons with an energy of ≤ 10 keV do appear (a), and oscillograms of the intensity of the X-ray emission from the ensemble of nanoparticles (b). In real time, the X-ray yield on channels 1 and 3 is delayed (by ~ 40 ns) due to the diffusion of quanta (≤ 10 keV) in comparison with the harder X-ray signal (channel 2), which escapes instantly (for comparison with the signals on channel 1 and 3 in real time, the maximum of the hard X-ray signal should be shifted to the left by ≈ 35 ns).

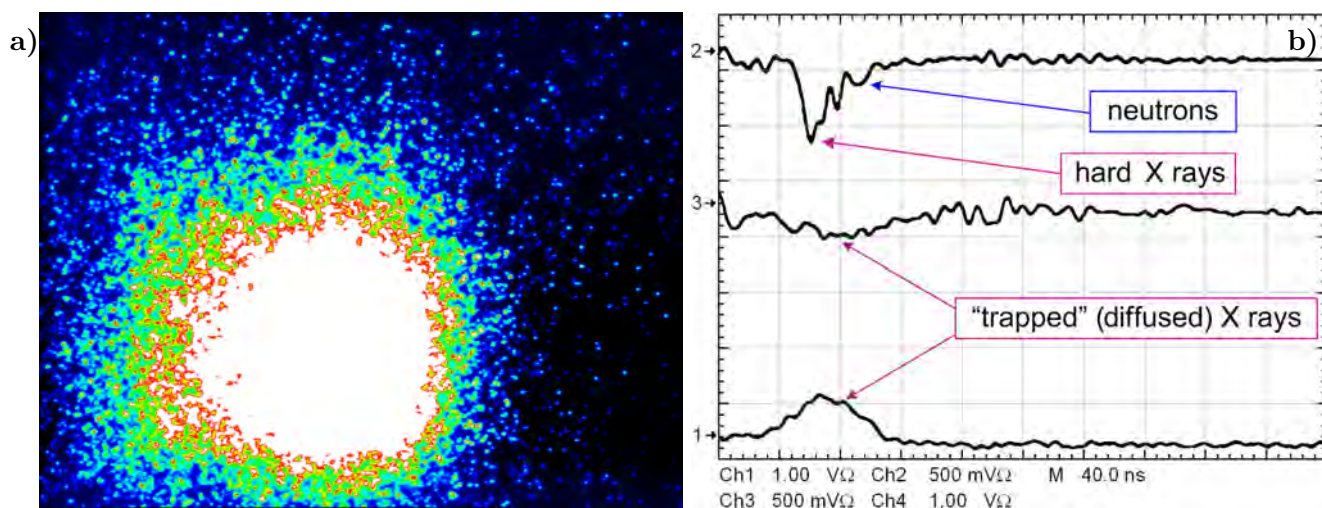


Fig. 4. Dynamics of X-ray yield in mode 3; here, CCD image of a self-organized cluster ensemble with a very low X-ray yield with an energy of 3–10 keV (a) and oscillograms of the X-ray and neutron yield intensity (b) (compare with signals in channels 1 and 3 presented in Fig. 2 b).

ensemble of the “ball” type (Figs. 1 b and 4 a) turns out to be quite sufficient for a clear registering of the image of the medium by a CCD camera. As a result, comparing the intensities of the oscillograms for mode 1 (Fig. 2) and mode 3 (Fig. 4), we found that a denser ensemble emits longer, but less intense radiation than a low-density ensemble (Fig. 2). Note that the sensitivity of channel 3 (Fig. 4 b) is twice that in Fig. 2 b. A very low X-ray intensity in channel 3 means that there is almost no X-ray output upward towards PIN-diode 3. Note that even harder X rays are also weakened and partially blocked by

dense inter-electrode ensembles (channel 2 in Figs. 3 and 4).

Modeling of the mechanisms of collective ion acceleration in the inter-electrode medium of the NVD was carried out by the particle-in-cell 2D simulations within the framework of the full electrodynamic code KARAT [15–20], which made it possible to clarify both the mechanism of collisional nuclear DD fusion and the generation of X rays in NVD. In particular, the results of 2D-modeling the dynamics of all particles in the discharge for the experimental geometry of electrodes and discharge parameters recognize the fundamental role of the formation of a virtual cathode in a complex anode plasma (Fig. 5). The VC is formed in front of the anode (inside the anode space, Fig. 5 a) due to the commutative convergence to the discharge axis Z of counter-propagating beams of quasirelativistic electrons drawn by the applied field from the inner walls of the conical part of the hollow cathode (from the region $r = 0.4–0.6$ cm; Fig. 5).

Coming back to the X-ray generation mechanism, let us turn to Fig. 5, which shows an example of modeling of a virtual cathode formation in an NVD. If we mentally place an inter-electrode ensemble of nanoparticles (in the form of a “ball,” such as that shown in Fig. 5 a) with a radius of $R \leq 0.35–0.4$ cm on the path of acceleration and deceleration of energetic electrons and deuterons (Fig. 5 a, b), then the main mechanism of X-ray generation in NVD becomes more clear. In fact, energetic electrons (up to 60 keV) interacting with the polydisperse medium of metal nanoclusters are losing energy, producing Bremsstrahlung and characteristic X-ray radiation.

With a decrease in the size of clusters in the ensemble, it is the surface properties that begin to dominate [17]. Therefore, the branched surface of nanoclusters in a stochastic ensemble with multiple scattering of photons at small angles can provide the condition $l_{SC} < R$ (at angles close to grazing ones). It is worthy to emphasize that nanoparticles at inter-electrode ensembles are nanocrystals of various sizes and structures and, as a result, reflect the X ray rather well [28]. The specific role of exact Bragg reflection and scattering inside a dense ensemble in the process of X-ray diffusion, as well as X-ray reflection, as a whole by shells from the outer layers of cold nanocrystals, “trapping” X rays inside stochastic ensembles is quite clear qualitatively but requires modeling and further analysis.

At the same time, in modes where the densities of inter-electrode ensembles are not as high as for shots with an anode of 13 Pd tubes (Figs. 1 b, 3, and 4) but smaller, as in the case of an anode with three Pd tubes (Fig. 2), the X-ray radiation comes out freely (here $l_{SC} \gg R_{eff}$), and the X-ray peak width turns out to be approximately proportional to the density of inter-electrode ensembles irradiated with electron beams. Indeed, the experiment shows that the larger the number of nanoclusters of the inter-electrode medium falling under the irradiation of energetic electrons, the more noticeable the yield of X-ray radiation with the same intensity. Modes 4 and 5 shown below in Figs. 6 and 7, respectively, illustrate this feature. The release of the X-ray radiation from the stochastic inter-electrode ensembles that are transparent for X rays make up a significant fraction of all shots fired with an anode of three Pd tubes at a pressure of $\sim 10^{-6}$ mbar.

It is interesting that, under certain conditions and sufficiently high densities of stochastic inter-electrode ensembles, the tendency for a larger X-ray yield with increasing ensemble density can sometimes be violated by some exceptions. In particular, even with a small number of Pd tubes in the anode (in regimes such as those shown above in Figs. 2, 6, and 7), cases of almost complete trapping of the X-ray radiation with subsequent bursts of a slightly different nature can be observed [17] (the latter regimes are discussed in the future paper). Indeed, mode 5 (Fig. 7) was obtained at a pressure of 10^{-6} mbar in the discharge chamber. At practically the same pressure, a regime with a self-organized dense ensemble (like an irregular “ball” in Fig. 8 a) with a very low X-ray release was registered not only with energies less

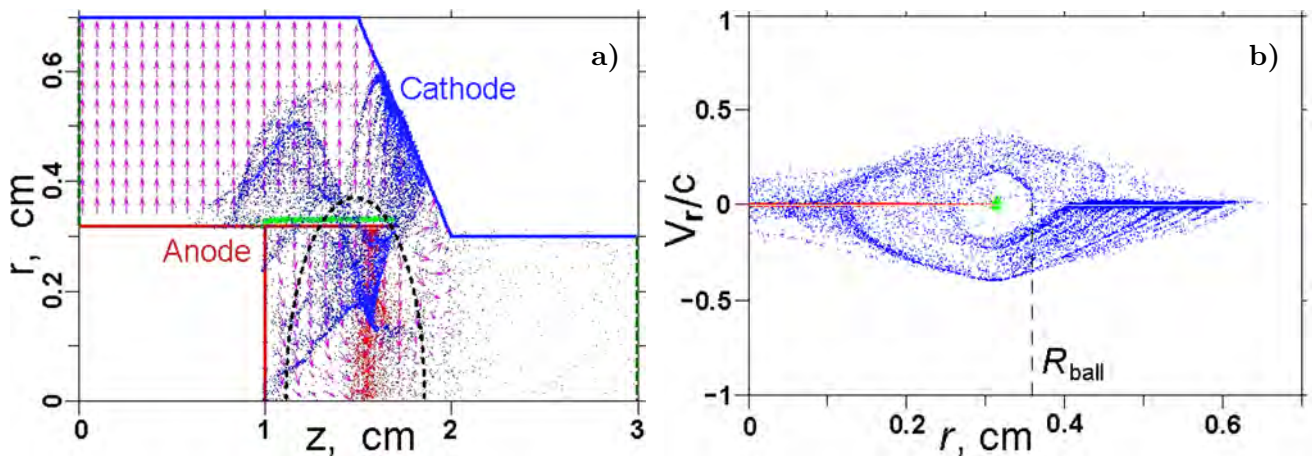


Fig. 5. Geometry of the discharge in PiC simulation at 25 ns (a) where the anode is shown in red and the cathode, in blue; also anode erosion “plasma” with deuterons is green. Blue points are quasirelativistic beam electrons emitted by the cathode under the action of an applied field, red points are fast ions accelerated by the VC field towards the Z axis. The dotted line shows the contour of an irregular “ball” of nanoclusters. The phase portrait of all particles typical for a formed cylindrical virtual cathode in the region $r \sim 0.1$ cm at the time moment 30 ns (b), where V_r is the radial velocity of particles, and c is the speed of light. The dotted line shows the radius of the “ball” of nanoclusters $R_{ball} \approx 0.37$.

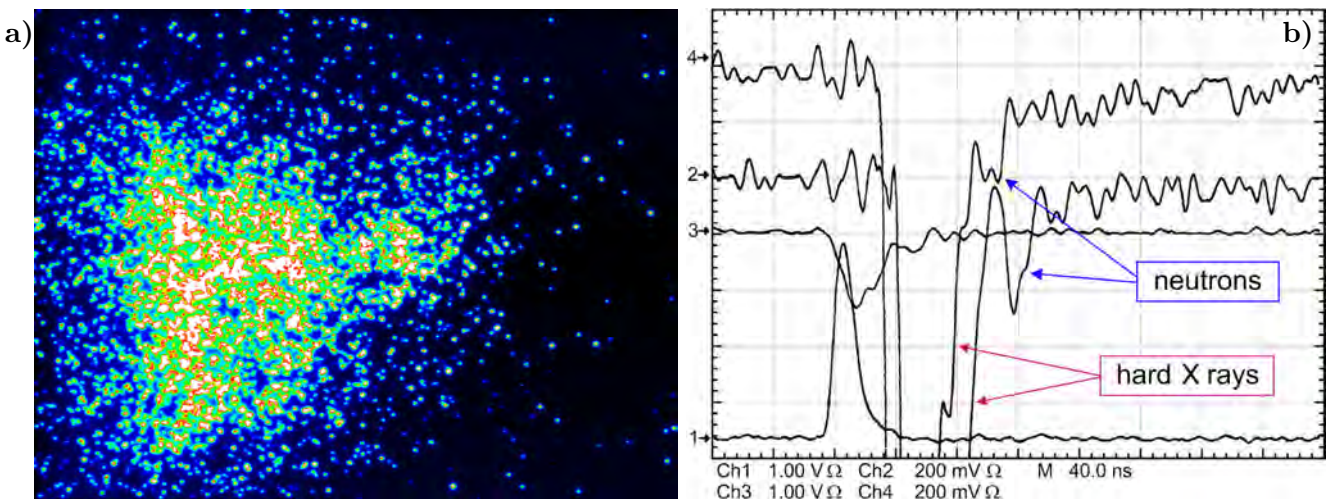


Fig. 6. Dynamics of the X-ray release in mode 4; here, CCD image of the inter-electrode medium (a) and oscillograms of the X-ray yield (b), when there is a strong flash of hard X ray (channels 2 and 4), with the sensitivity of channels 2 and 4 being much higher than on the oscillograms in Figs. 1–4; it is 200 mV.

than or ~ 10 keV (channels 1 and 3 in Fig. 8 b) but also in the harder part of the spectrum (channels 4 and 2). Here, fortunately, the signal on channel 1 turned out to be higher than the trigger U_{trig} , and we obtained oscillograms with sufficiently complete information on the large yield of DD neutrons and the “trapping” of the X-ray radiation by the self-organized inter-electrode ensemble. This mode, like those presented earlier in Figs. 2, 6, and 7, was obtained by firing also with an anode of three Pd tubes.

Usually, modes with a more saturated CCD image of a dense inter-electrode medium (such as Fig. 8 a) and with a well-defined virtual cathode, as in the case of an anode with three Pd tubes, also correspond to a more noticeable neutron yield due to the “dust stopping” of deuterons in a dense cluster medium, m.e.,

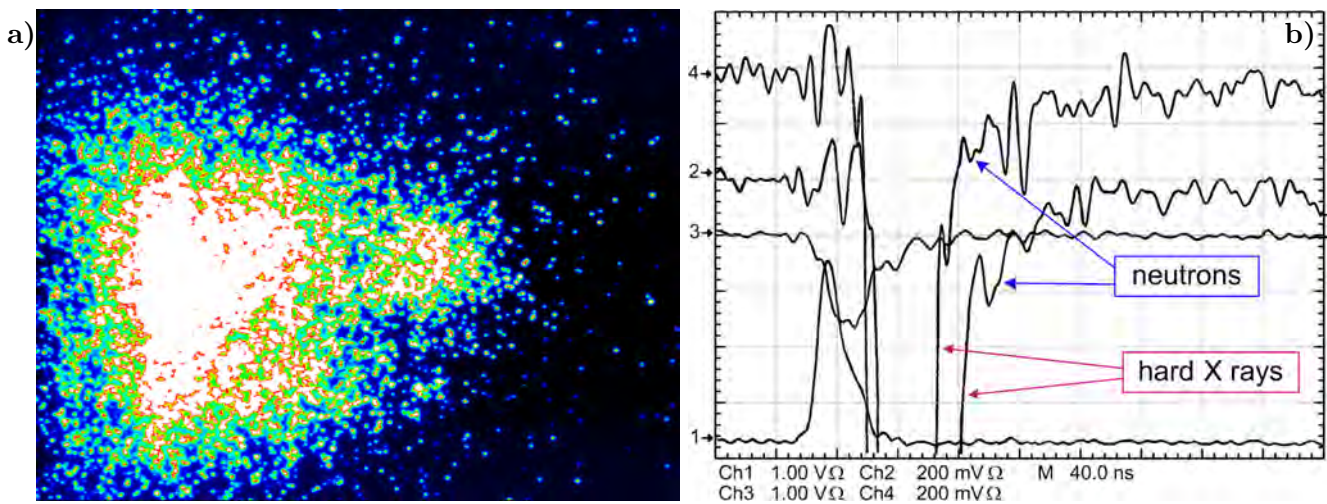


Fig. 7. Dynamics of the X-ray yield in mode 5; here, CCD image of the inter-electrode medium, which is somewhat denser than in mode 4 (Fig. 6) (a) and oscillograms of the X-ray radiation release (b) with a strong flash of hard X rays (channels 2 and 4), where the sensitivity of channels 2 and 4 is 200 mV.

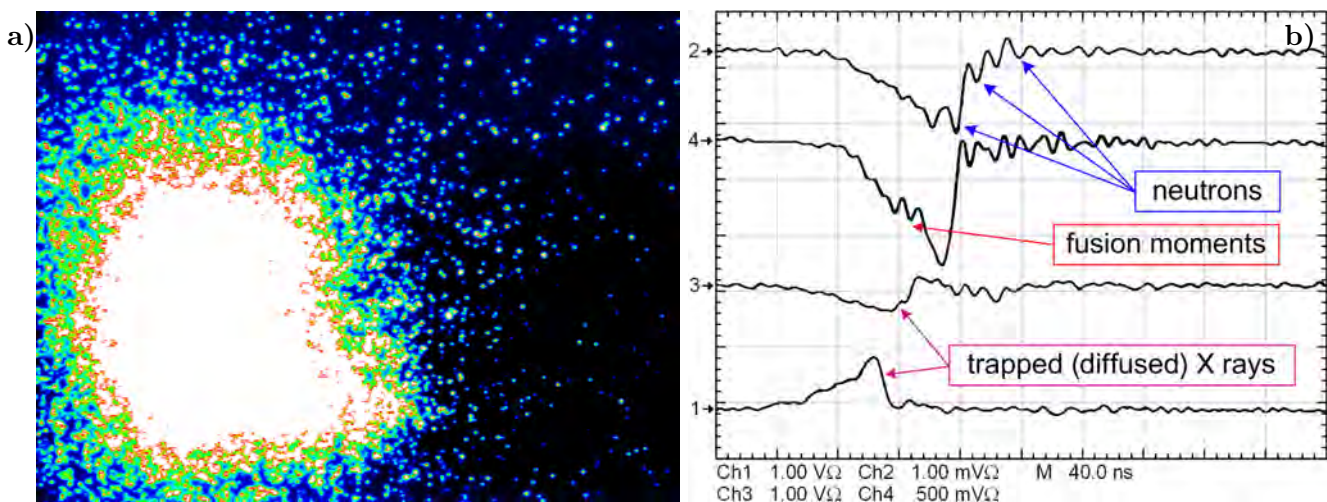


Fig. 8. Dynamics of the X-ray yield in mode 6; here, CCD image of dense and partially self-organized inter-electrode cluster ensemble (complex plasma microreactor [14–18]) (a) and oscillograms of X-ray yield (channels 1, 3, and 4) and neutron yield (channel 2) for specific ensemble with trapped deuterons and diffused (trapped) rather hard X rays (0.5 mm Cu before PM2; channel 2 sensitivity is 1 V and channel 4 sensitivity is 500 mV) (b).

additional DD fusion channel: “accelerated deuteron – deuterium-containing cluster.” The presence of several neutron peaks (Fig. 8 b, channel 2), i.e., the pulsating yield of DD neutrons indicates oscillations of deuterons in a potential well which is filled with deuterium-containing clusters. Thus, as the experiment shows, sufficiently self-organized ensembles of the type shown in Fig. 8 a practically “trap” both fast ions and rather hard X-ray radiation.

Note that earlier, detailed experimental data on the structure of Pd nanoclusters were obtained independently, in particular, on various well-defined types of crystal lattice depending on the size of Pd nanoclusters [28]. The same paper presents and discusses the diffraction properties of Pd nanoclusters, from which one can conclude that they can be quite good Bragg reflectors. Apparently, in dense

inter-electrode ensembles of Pd nanocrystals, easily reproducible and formed, as a result of erosion of Pd tubes under the influence of beams of energetic electrons, the near-surface layers of randomly oriented nanocrystals effectively form something like a distributed X-ray “mirror” resembling ring X-ray reflectors [3] (or distributed Bragg structures [29]). Near the surface of dense ensembles, chains of bright points were sometimes observed, closed on the X-ray “ball” itself or on the adjacent anode, i.e., a kind of localization of X rays [14–18]. Numerous studies in recent years of small-angle grazing incidence X-ray scattering (GISAXS) on 3D arrays of nanoparticles (see, for example, [30,31]) show that such arrays can be noticeable Bragg reflectors; this fact also indirectly confirms the possibility of the presence of the same properties in a dense inter-electrode cloud of Pd nanocrystals.

4. Concluding Remarks

Summarizing the above, we note that discharges with a Pd anode of three tubes are distinguished by the presence of a clear virtual cathode (like in Fig. 5), rather rare X-ray “trapping” modes (Fig. 8), and a high intensity of X-ray radiation in flares for not too dense ensembles (Figs. 2, 6, and 7). In the case of a 13 tube Pd anode, we often recorded rather dense inter-electrode ensembles (Figs. 1 b, 3, and 4) and, accordingly, good trapping of the X-ray radiation (~ 10 keV) and a low yield of diffuse X rays from the surface of the ensembles. But at the same time, due to the large number of Pd anode tubes densely located along the perimeter of the anode edge, the electron beams cannot freely penetrate into the anode space. In this case, we have a poorly formed VC, poor pumping of the ensemble by the energetic electron beams, and, as a consequence, the absence of X-ray bursts. Note that the X-ray yield in a discharge with a Pd anode in three spectral intervals measured, using the Ross filter method [32], is given in [33]. It can be seen from the histograms of the X-ray yield [33] that the X-ray spectra contain both the K_α -Pd line and transitions from higher levels for lower energies (of the L_α -Pd type), as well as a noticeable part of Bremsstrahlung with energies in the range of 30–55 keV.

Thus, the deceleration of energetic electrons in a polydisperse stochastic medium of an erosive anode plasma of a nanosecond vacuum discharge is accompanied by the generation of hard X-ray radiation. We experimentally found that, depending on the density of the polydisperse medium, the X rays (~ 10 keV and less) can either freely escape or be partially “trapped” by the inter-electrode medium and delayed in it, passing into a diffuse mode, if the density of cluster ensembles turns out to be high enough. Moreover, dense self-organized ensembles can also trap harder X rays, for example, K_α -Pd, 21.177 keV (Fig. 8), and the specifics of the further X-ray escape in such cases are of great interest. In fact, due to rescattering in dense polydisperse ensembles of nanoparticles (nanocrystals), when the X rays are trapped, conditions for stochastic feedback arise. It seems that the formation of such dense inter-electrode ensembles in NVD opens up certain prospects for the implementation of a random laser [4] in hard X-ray range [3], which was previously considered impossible due to the small scattering cross-section for X rays [22]. However, as shown in our future paper, despite a certain outward similarity, the nature of X-ray bursts from dense inter-electrode ensembles (like one presented in Fig. 8 a) is still different from a stochastic laser.

Acknowledgments

Yu. K. K. would like to thank Dr. Ives Vitel, former Director of Dense Plasma Lab, University P&M Curie, Paris for hospitality and strong support of scientific exchange and collaboration with Dr. Maurice Scowronek (DPL) at the very initial stage of this work.

References

1. J. C. Lindon, G. E. Tranter, and D. W. Koppenaal, (Eds.), *Encyclopedia of Spectroscopy and Spectrometry*, Elsevier (2017), 3rd ed.
2. R. Schoenlein, Th. Elsaesser, K. Holldack, et al., *Philos. Trans. A: Math. Phys. Eng. Sci.*, **377**, 20180384 (2019).
3. C. Elton, *X-Ray Lasers*, Academic Press, New York (1990).
4. V. S. Letokhov, *Zh. Éksp. Teor. Fiz.*, **53**, 1442 (1968) [*Sov. Phys. JETP*, **26**(4), 835 (1968)].
5. D. S. Wiersma, *Nat. Phys.*, **4**, 359 (2008).
6. H. Cao, *J. Phys. A: Math. Gen.*, **38**, 10497 (2005).
7. M. Noginov, *Solid State Random Laser*, Springer Series in Optical Science (2005), DOI: 10.1007/b106788.
8. G. H. Miley and S. K. Murali, *Inertial Electrostatic Confinement (IEC) Fusion*, Springer, New York (2014).
9. O. A. Lavrent'ev, *On the History of Thermonuclear Synthesis in the USSR*, Kharkov Physical Technical Institute, Kharkov, Ukraine (2012), 2nd ed. [in Russian].
10. W. C. Elmore, J. L. Tuck, and K. M. Watson, *Phys. Fluids*, **2**, 239 (1959).
11. R. A. Nebel and D. C. Barnes, *Fusion Technol.*, **38**, 28 (1998).
12. J. Park, R. A. Nebel, S. Stange, and S. K. Murali, *Phys. Plasmas*, **12**, 056315 (2005).
13. E. G. Evstatiev, R. A. Nebel, L. Chacon, et al., *Phys. Plasmas*, **14**, 042701 (2007).
14. Yu. K. Kurilenkov, M. Skowronek, and J. Dufty, *J. Phys. A: Math. Theor.*, **39**, 4375 (2006).
15. Yu. K. Kurilenkov, V. P. Tarakanov, S. Yu. Gus'kov, et al., *J. Phys. A: Math. Theor.*, **42**, 214041 (2009).
16. Yu. K. Kurilenkov, V. P. Tarakanov, V. T. Karpukhin, et al., *J. Phys.: Conf. Ser.*, **653**, 012025 (2015).
17. Yu. K. Kurilenkov, V. P. Tarakanov, S. Yu. Gus'kov, et al., *J. Phys.: Conf. Ser.*, **653**, 012026 (2015).
18. Yu. K. Kurilenkov, V. P. Tarakanov, S. Yu. Gus'kov, et al., *J. Phys.: Conf. Ser.*, **1147**, 012103 (2019).
19. V. Tarakanov, *User's Manual for Code KARAT*, Berkeley Research Associates Inc., Springfield, USA (1992).
20. V. Tarakanov, *EPJ Web Conf.*, **149**, 04024 (2017).
21. N. M. Lavandy, R. M. Balachandran, A. S. L. Gomes, and E. Sauvain, *Nature*, **368**, 436 (1994).
22. H. Cao, *Opt. Photon. News*, **16**, 24 (2005).
23. H. Cao, "Random laser – physics and application," Contribution to the Workshop on Coherent Phenomena in Disordered Optical Systems, Trieste, Italy, 26–30 May, 2014.
24. V. S. Letokhov, *Quantum Electron.*, **32**, 1065 (2002).
25. A. Yu. Varaksin, *High Temperature*, **56**, 275 (2018).
26. A. Yu. Varaksin, *High Temperature*, **57**, 555 (2019).
27. Yu. K. Kurilenkov, V. P. Tarakanov, V. T. Karpukhin, et al., *J. Phys.: Conf. Ser.*, **946**, 012025 (2018).
28. M. Suleiman, C. Borchers, M. Guerdane, et al., *J. Phys. Chem.*, **223**, 169 (2009).
29. J. Huang, M. M. Morshed, Z. Zuo, and J. Liu, *Appl. Phys. Lett.*, **104**, 131107 (2014).
30. K. Vegso, P. Siffalovic, M. Benkovicova, et al., *Nanotechnology*, **23**, 045704 (2012).
31. L. Chitu, P. Siffalovic, E. Majkova, et al., *Meas. Sci. Rev.*, **10**, 162 (2010).
32. P. A. Ross, *Phys. Rev.*, **28**, 425 (1926).
33. A. V. Oginov, Yu. K. Kurilenkov, and I. S. Samoilov, *J. Phys.: Conf. Ser.*, **1147**, 012081 (2019).